2024 International Conference on Space Robotics (iSpaRo)
June 24-27, 2024, Luxembourg

Characterization of a Rotating Magnetic Dipole Field for Contactless Detumbling of Space Debris

Travis J. Allen, Adam J. Sperry, Nicholas R. Posselli, Benjamin A. Minor, and Jake J. Abbott

2024 International Conference on Space Robotics (iSpaRo) | 979-8-3503-6723-2/24/$31.00 ©2024 IEEE | DOI: 10.1109/iSpaRo60631.2024.10687552

***Abstract*— There is a need for the remediation of space debris, but many objects must be detumbled before they can be safely serviced. In this paper, we describe an empirical study that is the first to evaluate the detumbling performance of a rotating magnetic dipole (MD) field. We develop a new rotating-permanent-magnet robotic end-effector capable of generating a strong MD field that can be rotated at high speeds. We construct a low-friction experimental apparatus to simulate a tumbling object. We conduct detumbling experiments using a rotating MD field with a variety of angular velocities, as well as the same field held static in two canonical orientations. We provide an estimate of the expected performance of each method in the microgravity environment of space by correcting our data for the friction in our experimental apparatus. We find that a rotating MD field detumbles an object in finite time, whereas a static field only detumbles an object asympotically to zero angular velocity. We find that the rotating MD field substantially outperforms a static MD field in reaching approximately zero angular velocity, provided the angular velocity of the rotating MD exceeds a modest minimum value. Finally, we observe a diminishing return in performance as we continue to increase the angular velocity of the rotating MD field.**

I. INTRODUCTION

The presence of debris in Earth's orbit poses a significant risk to human activity in space. By their very nature, debris are uncontrolled, uncooperative satellites or other resident space objects (RSOs) tumbling about arbitrary axes. In 1978, NASA scientist Donald Kessler proposed that a hazardous population of small debris would grow exponentially as a result of collisions in low Earth orbit, even if the addition of new human-made material were to halt [1]. This problem has since been termed the "Kessler syndrome", and it has been shown that for semi-synchronous and geosynchronous orbit altitudes this threshold has already been passed [2]. To prevent future disaster, debris will have to be recycled or removed from Earth's orbit [3].

In order for an RSO to be safely captured by a servicing craft, it is desirable that the RSO first be "detumbled", meaning decelerated to the point that its angular velocity with respect to the servicing craft is near zero [4]–[6]. Many groups have proposed detumbling strategies, which can be broadly characterized by whether or not the method relies on physical contact between the servicing craft and the RSO.

Contact-based methods have received much attention, but their application is limited to RSOs whose tumbling rate is below $30\,\mathrm{deg}\cdot\mathrm{s}^{-1}$ [5] (*i.e.*, below 0.0833 Hz), and they inherently carry a higher risk of collision between the RSO and servicing craft. In some cases, the tumbling rate of an RSO or the collision risk between the object and the craft may be too high to be deemed acceptable, which necessitates the development of contactless detumbling methods.

Perhaps the most promising suite of non-destructive, contactless detumbling methods includes those which rely on the torques induced in conductive nonmagnetic objects by externally applied magnetic fields. These methods, herein referred to as eddy-current detumbling methods, rely on a servicing craft's ability to generate magnetic fields that induce eddy currents in an object that is nonmagnetic but electrically conductive, which in turn induces a force-torque wrench on the object as the eddy currents interact with the magnetic field that generated them [7]–[10]. There exist two broad categories into which eddy-current detumbling methods may be grouped: those whose magnetic field is static in the spacecraft frame, and those whose magnetic field is dynamic in the spacecraft frame. Yongquist et al. [11] offer a thorough study of the detumbling ability of several static magnetic fields. They found that, for a spherical shell rotating slowly in a uniform magnetic field, the angular velocity of the sphere decays exponentially with time (as we might expect from first principles). To validate their analysis, they suspended a hollow aluminum sphere from a torsional pendulum and measured the angular velocity of the sphere over time, given some initial torsion. They tested the detumbling performance of a uniform magnetic field, the field of a single-coil electromagnet, and that of a rare-earth permanent magnet.

Our group recently showed that six-degree-of-freedom (6-DOF) manipulation of conductive nonmagnetic objects is possible using multiple magnetic field sources generating rotating magnetic dipole (MD) fields about controllable axes [12]. Our previous modeling efforts have described the force-torque wrench induced on a conductive, nonmagnetic, solid sphere in a quasistatic sense (*i.e.*, the sphere is approximately stationary in the world frame) [12]; these physics and models were later used to create a tractor-beam-like pulling effect [13], and they were adapted to manipulate nonspherical objects [14]. The object velocities present in the manipulation experiments of [12]–[14] have been small enough that the quasistatic assumption is valid, *i.e.*, the model was sufficient to form the foundation for successful closed-loop control of the objects' 6-DOF pose. However, such a quasistatic model may be insufficient in describing the force-torque wrench induced on a tumbling RSO.

This work was supported by the Air Force Research Laboratory, AFWERX, AFRL/RGKB under Contract Nos. FA9453-22-C-A043 and FA9453-22-C-A044. *(Corresponding author: T. J. Allen.)*

The authors are with the Department of Mechanical Engineering and the Robotics Center, University of Utah, Salt Lake City, UT 84112 USA {travis.allen,jake.abbott}@utah.edu

In this paper, we describe an empirical study that is the first to evaluate the detumbling performance of a rotating MD field, which we directly compare to the performance of the same magnetic field held static. We develop a new rotating-permanent-magnet robotic end-effector capable of generating a strong magnetic-dipole field that can be rotated at high speeds. We construct a low-friction apparatus to simulate a tumbling object in 1-DOF, and implement a Kalman filter to estimate the angular velocity and angular acceleration of the object. We conduct a detumbling experiment considering a rotating MD field with a variety of angular velocities and a static field at two canonical orientations. Finally, we provide an estimate of the expected performance of each method in the microgravity environment of space by correcting our data for the friction in our experimental apparatus.

II. METHODS

A. Experimental Apparatus

Experiments were conducted with the apparatus shown in Fig. 1. It comprises a magnetic end-effector mounted to a 6-DOF robot arm (Universal Robots UR5e), which acts on an aluminum sphere mounted in a 1-DOF tumbling rig.

The magnetic end-effector comprises a grade-42 NdFeB diametrically magnetized cylindrical permanent magnet with 50.8-mm outer diameter and length, and a 6.35-mm inner diameter (K&J Magnetics, RY04Y0DIA), mounted on a shaft that is supported on both ends by rolling element bearings. The magnet's dipole moment has a magnitude of $\|\boldsymbol{m}\| = 102.5\,\mathrm{A{\cdot}m^2}$. The magnet is connected to a brushed DC motor (Portescap 35GLT2R82-234E.1) with a belt-drive transmission, such that every rotation of the permanent magnet corresponds to 1.5 rotations of the motor and its incremental optical encoder (Portescap E9, 500 lines per revolution). The field of the magnet is sensed by an array of four Hall-effect sensors (Texas Instruments DRV5055A3ELPGQ1). The motor is driven using a servo driver (Advanced Motion Controls DPRALTE-020B080) and may be operated in velocity and position control modes. The servo driver is connected to a variable-voltage power supply (Mean Well UHP-1000-36) set to 43.0 V.

When viewed from at least 1.5 minimum-bounding-sphere radii away from its center, a diametrically magnetized cylindrical permanent magnet of approximately equal length and diameter can be accurately approximated as a point dipole $\boldsymbol{m}$ (units $\mathrm{A{\cdot}m^2}$) at position $\mathscr{P}_{\boldsymbol{m}}$, which generates a magnetic field vector $\mathbf{b}$ (units T) at each position $\mathscr{P}_{\mathbf{b}}$ in space:

$$\mathbf{b} = \frac{\mu_0}{4\pi\|\boldsymbol{\rho}\|^3}\left(\frac{3\boldsymbol{\rho}\boldsymbol{\rho}^T}{\|\boldsymbol{\rho}\|^2} - I\right)\boldsymbol{m} \tag{1}$$

where $\boldsymbol{\rho} = \mathscr{P}_{\mathbf{b}} - \mathscr{P}_{\boldsymbol{m}}$ is the relative displacement vector (units m), I is the identity matrix, $\mu_0 = 4\pi \times 10^{-7}\,\mathrm{N{\cdot}A^{-2}}$ is the permeability of free space, and all vectors are expressed in a common frame of reference [15].

The tumbling rig comprises two parts: the simulated RSO (sRSO) and a support structure. The sRSO comprises a 75.9-mm-diameter solid sphere of 2011-T3 aluminum mounted in a plastic housing that is supported between two low-friction plastic-and-glass rolling element bearings. The plastic housing surrounding the aluminum sphere is held together with nylon screws. An incremental optical encoder disc with 45 windows is attached to the sRSO. The support structure suspends the bearings in two Delrin® supports such that the center of the aluminum sphere is 180 mm away from any conductive material, excluding the minuscule amount of conductive material present in the encoder. The sensing portion of the incremental optical encoder is rigidly mounted to the support structure, and it contains two photointerruptors whose signals are routed through LM393 comparators so that the encoder can be read by a Sensoray s826 DAQ card operating in `QUADX4` mode. One photointerruptor is mounted on dovetail ways so that the separation between the two photointerruptors can be finely adjusted to ensure proper quadrature encoding. In such a configuration there are 180 encoder counts for each revolution of the sRSO. The optical encoder is used as the input to a Kalman filter to estimate the angular velocity and angular acceleration, as described in Appendix I.

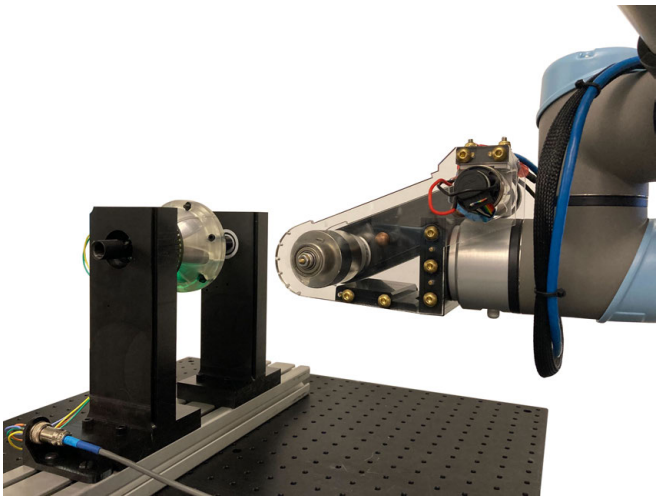

(a) Robot with magnetic end-effector (right) acting on a solid aluminum sphere held within a tumbling rig (left).

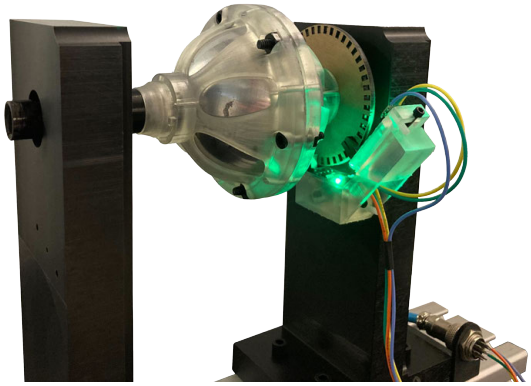

(b) Tumbling rig—comprising a support structure that allows for 1-DOF rotation with low friction, and an optical encoder to measure rotation—holding a solid aluminum sphere.

Fig. 1: Experimental apparatus.

B. Procedure

1) Collecting Experimental Data: To characterize the effect of rotating and static MD fields on detumbling the sRSO, the following procedure was implemented. First, the sRSO was brought to an initial angular velocity of $\omega = 6\,\text{Hz}$, using the magnetic end-effector placed in close proximity. Once the target initial angular velocity was reached, the end-effector was pulled away. Next, the permanent magnet was either commanded to rotate with some desired angular velocity $\omega_m := \|\boldsymbol{\omega}_m\|$, or to hold stationary with a desired dipole direction $\hat{\boldsymbol{m}}$. Then, the magnetic end-effector was placed in the desired configuration with respect to the sRSO: at a separation distance between the center of the sRSO and the center of the permanent magnet of $\|\boldsymbol{\rho}\| = 160\,\text{mm}$, with $\boldsymbol{\rho}$ orthogonal to, and with $\boldsymbol{\omega}_m$ parallel with, the rotation axis of the tumbling rig. The angle of the sRSO was then recorded by the optical encoder until the sRSO came to rest. Each such experiment was repeated for a total of five trials for each set of experimental parameters. We considered six nonzero values of ω_m, as well as two stationary configurations (*i.e.*, $\omega_m = 0$) with unique dipole directions: one in which the dipole points at the sRSO ($\hat{\boldsymbol{m}} \| \boldsymbol{\rho}$), and one in which the dipole is perpendicular to $\boldsymbol{\rho}$ ($\hat{\boldsymbol{m}} \perp \boldsymbol{\rho}$).

Additionally, the behavior of the tumbling rig with no applied magnetic field was recorded in the same manner. A complete description of the process by which the friction in the tumbling rig was characterized is given in Appendix II.

In postprocessing, the angular data was used to estimate the remaining two states of the sRSO according to the procedure in Appendix I. For each experimental configuration, the mean and its 95% confidence interval across the five trials were computed for each of the sRSO's three states. To account for transient errors due to initialization of our Kalman filter, we trimmed all of the data such that $\omega = 5.57\,\text{Hz}$ was viewed as the common initial angular velocity of all trials, which then defined the start of a trial.

2) Estimation of Behavior in Space: The procedure in Section II-B.1 accurately captures the behavior of the sRSO as it is detumbled on Earth while suspended by bearings in the tumbling rig. However, we wish to understand the behavior of the sRSO as if it were in the microgravity environment of space, *i.e.*, as if there were no friction due to the bearings or drag due to air. To achieve this, we first assumed that, in the region in which we are operating, the acceleration due to friction in the tumbling rig, α_f, can be approximated by a nonlinear, velocity-dependent three-parameter model:

$$\alpha_f(\omega) = -\gamma_0 \text{sgn}(\omega) - \gamma_1 \omega - \gamma_2 |\omega| \omega \tag{2}$$

The parameters of this model, γ_i, were identified by the procedure described in Appendix II. We then subtracted the portion of the acceleration of the sRSO due to friction from the total acceleration of the sRSO to reveal the acceleration that is due purely to the torque induced by the externally applied magnetic field, α_{mag}:

$$\alpha_{\text{mag}}(\omega) = \alpha(\omega) - \alpha_f(\omega) \tag{3}$$

where $\alpha(\omega)$ is the total acceleration of the sRSO in the tumbling rig. Finally, we numerically integrated $\alpha_{\text{mag}}(\omega)$ from an initial condition of 5.57 Hz to yield our best estimate of the angular velocity of the sRSO as a function of time if it were detumbled by the same means, but instead in the microgravity environment of space.

III. RESULTS

1) Experimental Results: The experimental results, as described in Section II-B.1, are shown in Fig. 2a. Let us first consider the performance of the static MD fields. We see that in both magnet orientations, $\hat{\boldsymbol{m}} \| \boldsymbol{\rho}$ and $\hat{\boldsymbol{m}} \perp \boldsymbol{\rho}$, the time taken to detumble the sRSO is less than the time taken to detumble when no magnetic field is present, indicating that the retarding torque induced by the combination of friction in the tumbling rig and the static MD fields is greater than that due to friction alone. We see that the time taken to detumble the sRSO is shorter for the $\hat{\boldsymbol{m}} \| \boldsymbol{\rho}$ configuration than it is for the $\hat{\boldsymbol{m}} \perp \boldsymbol{\rho}$ configuration.

Next, let us consider the results with the rotating MD fields. For all values of ω_m, the combination of the retarding torque induced by the rotating MD fields and by friction in the tumbling rig exceeds that due to friction in the tumbling rig alone, resulting in a shorter time-to-detumble than would occur without a magnetic field present. When $\omega_m = 0.5\,\text{Hz}$, the time-to-detumble due to the rotating MD field is shorter than the time-to-detumble due to the static MD field with $\hat{\boldsymbol{m}} \perp \boldsymbol{\rho}$, but longer than the time-to-detumble due to the static MD field with $\hat{\boldsymbol{m}} \| \boldsymbol{\rho}$. When $\omega_m = 3.5\,\text{Hz}$, the sRSO decelerations due to the rotating MD field and the static MD field with $\hat{\boldsymbol{m}} \| \boldsymbol{\rho}$ are initially approximately equal, but they gradually diverge as the sRSO's angular velocity decreases, with the rotating MD field providing greater decelerations at low values of ω, resulting in a shorter time-to-detumble. When $\omega_m > 3.5\,\text{Hz}$, a rotating MD field always outperforms any static MD field at any value of ω. As ω_m becomes larger, we find that the deceleration becomes more constant, resulting in $\omega(t)$ trajectories that appear more linear. As the rotating MD field is rotated faster than $\omega_m \approx 30\,\text{Hz}$, we find that an increase in ω_m is not accompanied by an appreciable decrease in the time-to-detumble, with the detumbling behavior due to $\omega_m = 30\,\text{Hz}$ and $\omega_m = 60\,\text{Hz}$ being almost indistinguishable from each other.

2) Estimated Results in Space: Finally, let us consider the estimated detumbling results in the microgravity environment of space, by correcting for friction in our tumbling rig as described in Section II-B.2, which are shown in Fig. 2b. We observe that the time-to-detumble is longer for every experimental configuration, but not equally so. When there is no applied magnetic field, the sRSO undergoes no deceleration, as we would expect. The times-to-detumble for the $\omega_m \geq 30\,\text{Hz}$ cases are only marginally longer than they are in the original experimental data, whereas the times-to-detumble for the $\omega_m = 0.5\,\text{Hz}$ case and both the static MD field cases are substantially longer than in the original experimental data. However, the trends noted in the original experimental data are maintained in this corrected data.

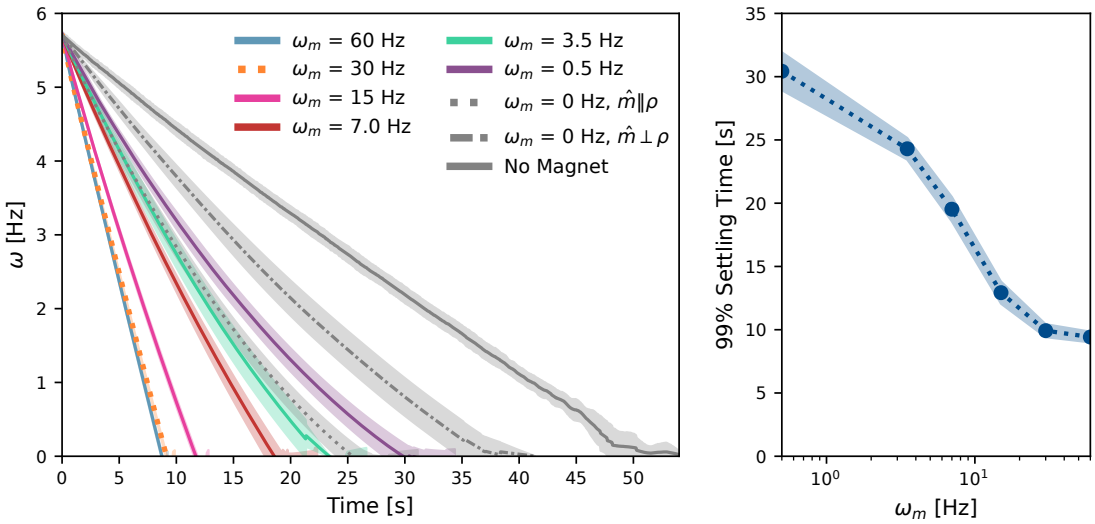

(a) Original experimental data.

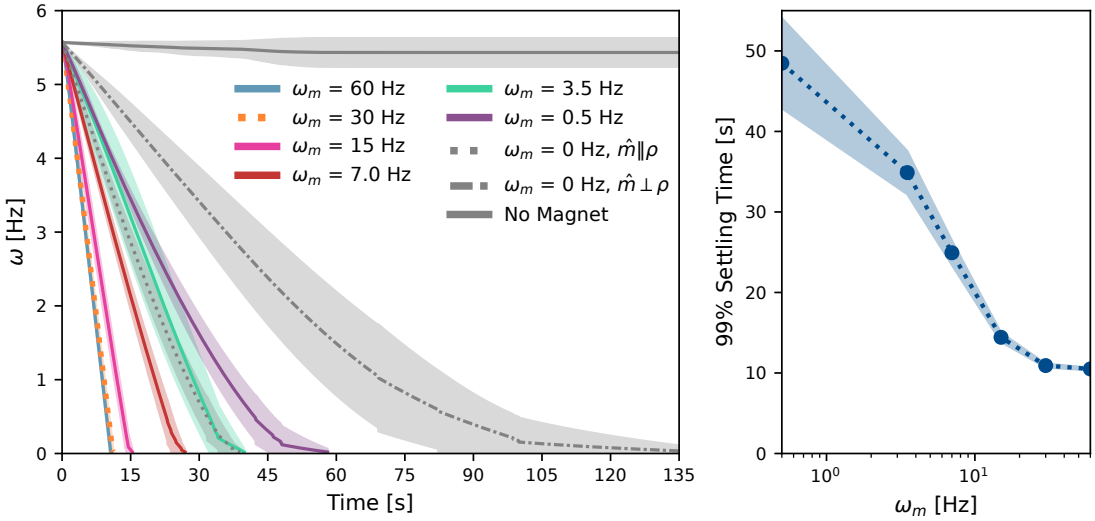

(b) Experimental data corrected to remove contribution of friction from the tumbling rig.

Fig. 2: Original and corrected experimental data of detumbling. Each curve shows the mean and its 95% confidence interval calculated from five runs. The numerical values reported are for the specific configuration tested, but the trends will generalize.

IV. DISCUSSION

When the applied magnetic field is static (*i.e.*, $\omega_m = 0$), the only source of change in magnetic flux in each differential element of the sRSO is the sRSO's angular velocity, $\boldsymbol{\omega}$. As $\boldsymbol{\omega}$ decreases, so too does the time-rate-of-change in magnetic flux, the resulting eddy currents, and the resulting sRSO deceleration. This process results in the asymptotic decay of the angular velocity of the sRSO, such that $\boldsymbol{\omega}$ does not reach zero in finite time—a result corroborated by the exponential decay model proposed by Yongquist *et al.* [11]. Our corrected results (Fig. 2b) using static MD fields also show these characteristic exponential decays (with the exception of the very end of the trials, at which point $\boldsymbol{\omega}$ becomes very small and the friction model for our tumbling rig seems to break down, with stiction likely becoming dominant).

According to (1), for a given dipole $\boldsymbol{m}$, at any given distance, $\|\boldsymbol{\rho}\|$, the magnitude of the field, $\|\mathbf{b}\|$, has a maximum when $\boldsymbol{\rho} \| \boldsymbol{m}$, which is twice as large as the minimum value, which occurs when $\boldsymbol{\rho} \perp \boldsymbol{m}$. Thus, in consideration of Faraday's law of induction, we should expect the currents induced in the sRSO to be larger in the $\boldsymbol{\rho} \| \boldsymbol{m}$ configuration than in the $\boldsymbol{\rho} \perp \boldsymbol{m}$ configuration; larger induced currents will produce stronger induced torques as the currents interact with the applied magnetic field, and consequently, will result in greater sRSO deceleration. This is exactly the behavior that we observe.

Unlike the exponential decay caused by static MD fields, a rotating MD field causes the sRSO to detumble to zero angular velocity in finite time. This is because a time-rate-of-change in magnetic flux is caused by the rotation of the field in addition to the rotation of the sRSO. Initially, increasing the value of $\boldsymbol{\omega}_m$ results in a larger sRSO de-

celerations. However, there appears to be an upper bound on the achievable deceleration, as the times-to-detumble for the $\omega_m = 30\,\text{Hz}$ and $\omega_m = 60\,\text{Hz}$ cases are nearly identical. This may indicate that, under our experimental operating parameters, the power-optimal value of ω_m for minimum-time detumbling lies somewhere near $\omega_m \approx 30\,\text{Hz}$.

We find that a very slowly rotating MD field (*i.e.*, $\omega_m = 0.5\,\text{Hz}$) outperforms a static MD field in the worst-case orientation, $\boldsymbol{\rho} \perp \boldsymbol{m}$, but underperforms a static MD field in a best-case orientation, $\boldsymbol{\rho} \| \boldsymbol{m}$. This behavior is somewhat expected, given that the sRSO experiences a time-averaged field strength that is less than the field experienced when $\boldsymbol{\rho} \| \boldsymbol{m}$ but more than the field experienced when $\boldsymbol{\rho} \perp \boldsymbol{m}$. However, we would still expect $\omega_m = 0.5\,\text{Hz}$ to result in detumbling in finite time, so it is unclear why the corrected data of Fig. 2b appears more like an exponential decay. This is left as an open question.

For high values of ω_m (*i.e.*, $\omega_m > 15\,\text{Hz}$), the contribution of the angular velocity of the sRSO to its deceleration appears to be negligible, as the slope of the curves in Fig. 2b are nearly constant in time. However, for smaller values of ω_m—*i.e.*, those for which ω_m and ω are of the same order of magnitude—we see that the contribution of the angular velocity of the sRSO to its deceleration is greater when ω is high, and decreases with decreasing ω, resulting in smaller sRSO decelerations that are due primarily to the contribution from the rotating MD field.

Finally, although we expect the trends in this study to hold generally, the quantitative values reported here should not be assumed to extrapolate to other configurations (*i.e.*, other objects, MD strengths, and distances between the object and the MD). A complete characterization of detumbling using a rotating MD field should be recast using dimensional analysis, such that the underlying physics can be expressed in a dimensionless fashion; this is left as an open problem. However, we anticipate that the scaling analysis would be similar to the dimensionless results from Pham *et al.* [12], which characterized induced force and torque on quasistatic objects due to rotating MD fields. For example, Pham *et al.* [12] found that magnetic torque scales with nondimensional distance $\propto (\|\rho\|/r)^{-6}$, where r is the radius of the spherical sRSO; we would expect that induced deceleration during detumbling would scale similarly.

Appendix I
State Estimation

We can construct a discrete-time state-space model of the sRSO, with sampling period T, in which the three states are the angle θ, angular velocity ω, and angular acceleration α, the exogenous input is the angular jerk η generated by the magnet (as well as by friction in our experimental device) on the sRSO, which is unknown to us and assumed to be constant from sample i to sample $i+1$:

$$\begin{bmatrix}\theta_{i+1}\\ \omega_{i+1}\\ \alpha_{i+1}\end{bmatrix} = \begin{bmatrix}1 & T & T^2/2\\ 0 & 1 & T\\ 0 & 0 & 1\end{bmatrix}\begin{bmatrix}\theta_i\\ \omega_i\\ \alpha_i\end{bmatrix} + \begin{bmatrix}T^3/6\\ T^2/2\\ T\end{bmatrix}\eta_i \tag{4}$$

Our goal is to estimate the sRSO's states throughout time, using data gathered by the incremental optical encoder on the tumbling rig. To accomplish this, we implement a Kalman filter. The Kalman filter assumes a discrete-time state-space model of the form

$$\boldsymbol{x}_{i+1} = \mathbb{A}_d \boldsymbol{x}_i + \mathbb{B}_d \boldsymbol{u}_i + \boldsymbol{w} \tag{5}$$

$$\boldsymbol{y}_i = \mathbb{C}_d \boldsymbol{x}_i + \mathbb{D}_d \boldsymbol{u}_i + \boldsymbol{v} \tag{6}$$

where $\boldsymbol{w} \sim \mathcal{N}(\boldsymbol{0}, \mathbb{W})$ and $\boldsymbol{v} \sim \mathcal{N}(\boldsymbol{0}, \mathbb{V})$ are zero-mean gaussian noise terms on the state updates and sensor updates, respectively [16]. $\mathbb{W}$ and $\mathbb{V}$ are positive-definite symmetric covariance matrices that encode the process model's and the observation model's noise levels, respectively. In our case, the incremental optical encoder is modeled as

$$\boldsymbol{y}_i = \begin{bmatrix}1 & 0 & 0\end{bmatrix}\begin{bmatrix}\theta_i\\ \omega_i\\ \alpha_i\end{bmatrix} + \begin{bmatrix}0\end{bmatrix}\eta_i + \boldsymbol{v} \tag{7}$$

It is easy to verify that the system is observable given $\mathbb{A}_d$ and $\mathbb{C}_d$ [17], so we may proceed with the design of the Kalman filter. At each discrete-time update, the Kalman filter moves forward in time to generate estimates of the states:

$$\tilde{\boldsymbol{x}}_{i+1|i} = \mathbb{A}_d \tilde{\boldsymbol{x}}_{i|i} + \mathbb{B}_d \boldsymbol{u}_i \tag{8}$$

$$\mathbb{P}_{i+1|i} = \mathbb{A}_d \mathbb{P}_{i|i} \mathbb{A}_d^T + \mathbb{W} \tag{9}$$

$$\mathbb{K}_{i+1} = \mathbb{P}_{i+1|i} \mathbb{C}^T (\mathbb{C}\mathbb{P}_{i+1|i}\mathbb{C}^T + \mathbb{V})^{-1} \tag{10}$$

$$\tilde{\boldsymbol{x}}_{i+1|i+1} = \tilde{\boldsymbol{x}}_{i+1|i} + \mathbb{K}_{i+1}(\boldsymbol{y}_{i+1} - \mathbb{C}\tilde{\boldsymbol{x}}_{i+1|i} - \mathbb{D}\boldsymbol{u}_{i+1}) \tag{11}$$

$$\mathbb{P}_{i+1|i+1} = \mathbb{P}_{i+1|i} - \mathbb{K}_{i+1}\mathbb{C}\mathbb{P}_{i+1|i} \tag{12}$$

Since we have no way to know the input, η_i, we simply assume $\eta = 0$ for all time. This is equivalent to an assumption that α changes relatively slowly, which is likely to be an accurate assumption except for at the very beginning of a detumbling run (at which point we expect an approximate step change in acceleration).

The observation noise was quantified by computing the residual error between the quantized signal that would be reported by the encoder and the actual angle of a theoretical sRSO tumbling at a constant speed that is slow relative to the encoder's sampling rate, which was concatenated into a $1 \times N_V$ array V, from which we compute:

$$\mathbb{V} = \frac{1}{N_V} V V^T \tag{13}$$

To estimate the process-noise matrix $\mathbb{W}$, the three diagonal terms were first manually tuned during postprocessing of data from a pilot study such that the estimated angle of the sRSO, θ, largely overlapped the encoder-measured angle. This initial Kalman filter was used to complete the process described in Appendix II, such that an initial model of the friction in the tumbling rig could be obtained. This model was then used in a numerical simulation of an sRSO starting from an initial condition of 6 Hz and whose only acceleration was that due to friction to create a time-series of state data, $\boldsymbol{x}_{\text{sim}}$. Next, state updates from the process model in (8) were computed at each $\tilde{\boldsymbol{x}}_{i|i} = \boldsymbol{x}_{\text{sim},i}$. This enabled us to compute an

TABLE I: Nominal System Parameters

Parameter	Value
γ_0	$0.638\,\mathrm{rad{\cdot}s^{-2}}$
γ_1	$5.41\times10^{-3}\,\mathrm{s^{-1}}$
γ_2	$1.21\times10^{-5}\,\mathrm{rad^{-1}}$

error between the process update, $\tilde{\boldsymbol{x}}_{i+1|i}-\tilde{\boldsymbol{x}}_{i|i}$, and the ground truth state update, $\boldsymbol{x}_{\mathrm{sim},i+1}-\boldsymbol{x}_{\mathrm{sim},i}$. There were N_W such computations, which were concatenated into a $3\times N_W$ matrix W such that the process-noise covariance matrix, $\mathbb{W}$, could be computed in a manner analogous to (13). The resulting $\mathbb{W}$ was used in the Kalman filter used in the experimental results of Fig. 2, as well as the final friction model of Table I and Fig. 3.

Appendix II
Characterization of the Tumbling Rig

To identify the nominal system parameters γ_i of (2), five trials were performed in which the sRSO started with an initial angular velocity of 6 Hz and was allowed to spin freely until coming to a rest. The system states were estimated and recorded using the procedure in Appendix I. The state estimator has transient behavior at initialization that produces data at the beginning of the trials that is not physically realistic. The data corresponding to this behavior were removed from each trial. The full data from the five trials are shown in Figs. 3a and 3b. The truncated data are shown in Fig. 3c, as is the fit of (2) found with the Levenberg-Marquardt algorithm. The model parameters for (2) are provided in Table I.

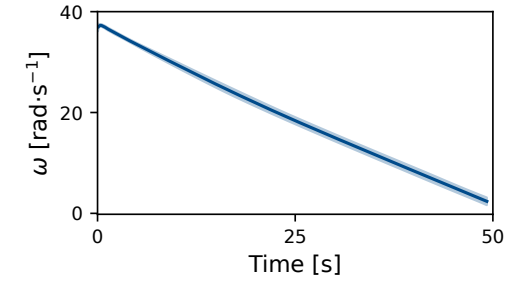

(a) Angular velocity vs. time.

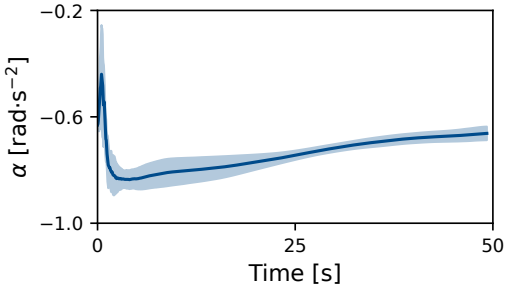

(b) Angular acceleration vs. time.

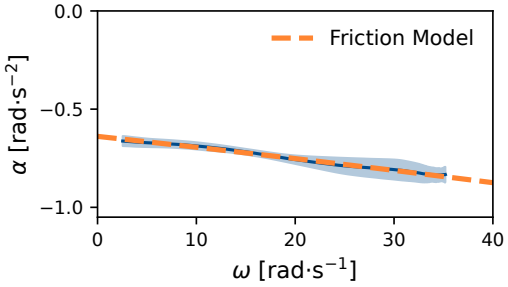

(c) Angular acceleration vs. angular velocity (blue) with best-fit friction model $\alpha_f(\omega)$ (orange).

Fig. 3: Characterization of friction in the tumbling rig. Each curve shows the mean and its 95% confidence interval calculated from five runs.

Acknowledgment

This project is a collaboration with Rogue Space Systems.

References

[1] D. J. Kessler and B. G. Cour-Palais, "Collision frequency of artificial satellites: The creation of a debris belt," *J. Geophys. Res. Space Phys.*, vol. 83, no. A6, pp. 2637–2646, 1978.

[2] D. J. Kessler, N. L. Johnson, J. Liou, and M. Matney, "The Kessler syndrome: implications to future space operations," *Adv. Astronaut. Sci.*, vol. 137, no. 8, p. 2010, 2010.

[3] T. J. Colvin, J. Karcz, and G. Wusk, "Cost and benefit analysis of orbital debris remediation," NASA Headquarters, Office of Technology, Policy, and Strategy, Tech. Rep., 2023.

[4] H. Hakima, M. C. F. Bazzocchi, and M. R. Emami, "A deorbiter CubeSat for active orbital debris removal," *Adv. Space Res.*, vol. 61, no. 9, pp. 2377–2392, 2018.

[5] M. Shan, J. Guo, and E. Gill, "Review and comparison of active space debris capturing and removal methods," *Prog. Aerosp. Sci.*, vol. 80, pp. 18–32, 2016.

[6] M. A. Nurge, R. C. Youngquist, R. A. Caracciolo, M. Peck, and F. A. Leve, "A thick-walled sphere rotating in a uniform magnetic field: The next step to de-spin a space object," *Am. J. Phys.*, vol. 85, no. 8, pp. 596–610, 2017.

[7] F. Sugai, S. Abiko, T. Tsujita, X. Jiang, and M. Uchiyama, "Detumbling an uncontrolled satellite with contactless force by using an eddy current brake," in *Proc. IEEE/RSJ Int. Conf. Intelligent Robots and Systems*, 2013, pp. 783–788.

[8] N. Ortiz Gómez and S. J. I. Walker, "Eddy currents applied to detumbling of space debris: Analysis and validation of approximate proposed methods," *Acta Astronaut.*, vol. 114, pp. 34–53, 2015.

[9] X. Liu, Y. Lu, Y. Zhou, and Y. Yin, "Prospects of using a permanent magnetic end effector to despin and detumble an uncooperative target," *Adv. Space Res.*, vol. 61, no. 8, pp. 2147–2158, 2018.

[10] X. Liu, Y. Lu, Q. Zhang, and K. Zhang, "An application of eddy current effect on the active detumble of uncontrolled satellite with tilt air gap," *IEEE Trans. Magn.*, vol. 55, no. 12, pp. 1–11, 2019.

[11] R. C. Youngquist, M. A. Nurge, S. O. Starr, F. A. Leve, and M. Peck, "A slowly rotating hollow sphere in a magnetic field: First steps to de-spin a space object," *Am. J. Phys.*, vol. 84, no. 3, pp. 181–191, 2016.

[12] L. N. Pham, G. F. Tabor, A. Pourkand, J. L. B. Aman, T. Hermans, and J. J. Abbott, "Dexterous magnetic manipulation of conductive nonmagnetic objects," *Nature*, vol. 598, pp. 439–443, 2021.

[13] D. K. Dalton, G. F. Tabor, T. Hermans, and J. J. Abbott, "Attracting conductive nonmagnetic objects with rotating magnetic dipole fields," *IEEE Robot. Autom. Lett.*, vol. 7, no. 4, pp. 11 484–11 491, 2022.

[14] G. F. Tabor, L. N. Pham, J. J. Abbott, and T. Hermans, "Adaptive manipulation of conductive, nonmagnetic objects via a continuous model of magnetically induced force and torque," in *Proc. Robotics: Science and Systems*, 2022.

[15] A. J. Petruska and J. J. Abbott, "Optimal permanent-magnet geometries for dipole field approximation," *IEEE Trans. Magn.*, vol. 49, no. 2, pp. 811–819, 2013.

[16] D. Simon, *Optimal state estimation: Kalman, H infinity, and nonlinear approaches*. John Wiley & Sons, 2006.

[17] C.-T. Chen, *Linear System Theory and Design*, 4th ed. Oxford University Press, 2012.